SLAC-TN-07-026

Introducing Defects in Photonic Band-Gap (PBG) Crystals

Elliott C. Johnson

Office of Science, Science Undergraduate Laboratory Internship (SULI)

North Dakota State University

Stanford Linear Accelerator Center

Stanford, CA

August 24, 2007

Prepared in partial fulfillment of the requirements of the Office of Science, Department of Energy's Science Undergraduate Laboratory Internship under the direction of Jim Spencer in the Advanced Acceleration Research Dept., Stanford Linear Accelerator Center.

Participant: _____

Signature

Research Advisor: _____

Signature

Work supported in part by US Department of Energy contract DE-AC02-76SF00515

TABLE OF CONTENTS

Abstract **ii**

I. Introduction **1**

II. Materials and Methods **2**

III. Results **4**

IV. Discussion and Conclusions **5**

VI. References **9**

VII. Acknowledgments **9**

References **9**

ABSTRACT

Introducing Defects in Photonic Band-Gap (PBG) Crystals. ELLIOTT C. JOHNSON (North Dakota State University, Fargo, ND, 58105) JIM SPENCER (Advanced Acceleration Research Dept., Stanford Linear Accelerator Center, Stanford, CA 94025)

Photonic Band-Gap (PBG) fibers are a periodic array of optical materials arranged in a lattice called a photonic crystal. The use of PBG fibers for particle acceleration is being studied by the Advanced Accelerator Research Department (AARD) at SLAC. By introducing defects in such fibers, e.g. removing one or more capillaries from a hexagonal lattice, spatially confined modes suitable for particle acceleration may be created. The AARD has acquired several test samples of PBG fiber arrays with varying refractive index, capillary size, and length from an external vendor for testing. The PBGs were inspected with a microscope and characteristics of the capillaries including radii, spacing, and errors in construction were determined. Transmission tests were performed on these samples using a broad-range spectrophotometer. In addition, detailed E-field simulations of different PBG configurations were done using the CUDOS and RSOFT codes. Several accelerating modes for different configurations were found and studied in detail.

I. INTRODUCTION

In order to study particle physics at smaller scales, higher accelerating gradients are needed. These can be created by using smaller structures, where larger field strengths should be generated. One such structure proposed by the Advanced Accelerator Research Department (AARD) at SLAC is a photonic band-gap (PBG) material with a hollow-core defect[1]. PBG crystals can be assembled by stacking glass capillary tubes in a tight lattice (see Fig. 1). It has been found that introducing central defects, e.g. eliminating one capillary spatially confines modes and equivalently longitudinal E-fields in the defect, creating an accelerator structure[1]. A particular configuration where the diameter of the central defect is 52% the spacing of outside capillaries is called the Lin configuration. The lowest accelerating mode for this configuration using a 1.3μ diameter defect has been studied in detail[1]. PBG fiber arrays can be constructed in very small sizes compared to the accelerator structures in current use, but none yet match the Lin configuration. Another potential benefit is their dielectric composition which allows control of phase velocity closer to the speed of light (SOL) and higher breakdown fields than metallic cavities.

To understand commercially available PBG crystals, samples formed with capillaries of varying wall thickness and radii were obtained from Incom, Inc[2]. With a microscope, the radii and spacing (pitch) of the capillary tubes were characterized for simulation to determine if accelerating modes will propagate in these samples. While PBG fibers are available from outside vendors, most commercial samples are primarily manufactured for telecom applications (TEM modes) and are not suitable for acceleration. For this reason, we are looking to assemble custom crystals based on the calculations and searches for available capillary tubes. This would provide a better means of understanding quality assurance, ease of making defects, and more efficient study of damage and coupling effects.

CUDOS MOF Utilities[3] and RSOFT's BandSOLVE[4] are two software codes used to simulate characteristics of PBG fibers. BandSOLVE is used to define the band gaps

for a given structure and to locate at which wavelengths the band gap overlaps the SOL line–a critical feature for particle acceleration. When the relevant wavelength regions are determined, CUDOS is used to find the precise frequencies of the accelerating modes, i.e. the TM_{0l}-like modes. Many parameters determine the allowed modes for acceleration, including the aforementioned radii and spacing, and also the refractive index of the material. With CUDOS, values for these parameters which lead to strong longitudinal E fields at unique wavelengths can be found–when they exist.

For our application, PBG crystals must be driven by a laser to achieve sufficiently-high gradients. The laser plays the role of the klystron in conventional RF accelerating cavities. The coupling of this field into the defect is a further major research problem. There is no commercial testing process available to us for this. To examine the transmission of our samples, we tested them with a spectrum of light, using a spectrophotometer.

II. MATERIALS AND METHODS

1. PBG Sample Characterization

The PBG crystal samples were inspected using a microscope with attached CCD camera and computer display. The sample was placed on a beam splitter. An external light illuminated the side of the beam splitter, which directed light upward through the sample and into the viewing lens. Several construction errors were photographed. For estimation of capillary diameter and spacing, segments of wires with known diameters were placed on the sample. Wires were also threaded into capillary tubes for further size approximation.

With the inner diameter of the capillaries and the pitch measured, the glass packing fraction (GPF), i.e. the ratio of the cross-sectional glass area to total area of the PBG sample was calculated. This was done by assuming the number of rings to be very large. Furthermore, Mathematica code was written to calculate the GPF for an arbitrary hexagonal configuration, by allowing the user to enter the inner and outer diameters of capillary tubes,

the number of rings removed constituting a defect, and the total number of rings.

A broad-range spectrophotometer[5] was used to measure the transmittance of each sample over the range 325 nm $\leq \lambda \leq$ 3000 nm. Baseline data was taken before adding the samples to quantify water impurities in the system, which absorb light in a frequency dependent way. Dry air was continuously pumped through the system to reduce such ambient effects and provide reproducibility.

2. PBG Mode Simulation

Table 1 shows a comparison of PBG configurations and our test samples (Incom A-D). Allowed bands for accelerating modes were found using RSoft's BandSOLVE[4]. BandSOLVE utilizes a CAD interface to construct fiber arrays. We constructed a 10-ring lattice (with no introduced defect) for the Lin configuration. We also made 10-ring lattices for the Incom B and D samples, scaled so that an introduced (single pulled tube) defect would be 5.0 μm in diameter. With each CAD lattice, a simulation was run that produced the set of band gaps for the configuration. A plot of the transition bands for the Lin fiber is given in Fig. 2 (with the SOL line also plotted for reference). The band gap diagrams for Incom Samples B and D are given in Fig. 3 and Fig. 4, respectively. Wavelengths that correlate to these bands were examined with CUDOS to search for acceptable accelerating modes.

Wavelengths corresponding to the SOL-crossing bands from the band diagram and the PBG parameters from Table 1 were entered into CUDOS MOF Utilities[3]. With these values and an effective index range, CUDOS uses the multipole method to find allowed modes[6]. For these simulations, the 6,8, or 8 ring cases were deemed adequate and saved time. Numerical information including the real and imaginary components of the effective index is given for found modes, as well as an executable for modal field visualization. The E_z field for the fundamental mode of the Lin fiber configuration[1] is shown in Fig. 5. By selecting a point on the mode cross-section, the relative intensity for that point of the mode

can be measured. The user is able to select viewing a Cartesian component of the Poynting vector, E or H field. The real, imaginary, or absolute part of the field can also be specified. In this way, the 2nd, 3rd, and 5th band gaps of the Lin configuration were studied, as well as the 2 lowest SOL-crossing bands for Incom samples B and D with a single pulled capillary defect.

III. RESULTS

1. PBG Sample Characterization

A comprehensive list of estimated parameters for the samples and other configurations is given in Table 1. The number of rings eliminated for the defect (N_{Def}) and the number of rings for calculation (N_{Rgs}) are unspecified for the Incom samples since these were to be determined in the study. Fig. 6 depicts an Incom PBG sample with a construction error that could be used as a single capillary defect. Other construction errors are shown in Fig. 7. A comparison of transmittance data for each sample as a function of wavelength is given in Fig. 8.

2. Found Modes

Five additional modes that may be suitable for acceleration were found for the Lin configuration. Fig. 9 shows a mode from Band Gap 3 (as shown in Fig. 2). Accelerating modes were found in the first and second SOL-crossing bands for Incom D, and these are shown in Figures 10 and 12. No defect modes were found for Incom B. One figure of merit is the ratio of maximum E_z in the core to the maximum of E_z in the glass. These ratios, the excitation wavelength, and the real and imaginary components of the effective index for each mode that was found are given in Table 2 for direct comparison with the lowest mode from the Lin configuration–referred to as the Lin mode[1].

IV. DISCUSSION AND CONCLUSIONS

1. PBG Characterization

Construction errors were observed on all Incom samples. The majority of these errors occurred along the boundary of a larger hexagonal lattice as shown in Fig. 7. This is likely due to a process of construction where groups of smaller hexagonal lattices are forced together to create a larger or super-lattice. The relative occurrence of errors corresponds to a construction "Quality" factor in Table 1. The Incom sample with significantly larger capillaries than the other samples showed very few construction errors, as expected.

Nearly all of the Incom samples had a smaller GPF (and thus larger % air) than the Lin configuration. This is a favorable result, as particle acceleration near c requires the overall refractive index of the lattice to be only slightly larger than 1. Unfortunately, it appears that on scales of capillary diameter $\leq$ 100 μm (Incom sample C excluded), there is a direct correspondence of lower GPF to construction errors due to manufacturing inexperience.

2. Transmission Test Data

The absorption by vibrational levels of water impurities is evident for all samples over the range $\lambda \geq$ 2700 nm as shown in Fig. 8. Absorption below $\lambda \approx 400$ nm for samples A and B implies borosilicate composition, because boron-induced defects in the silica absorb energy over this wavelength. For better quality glass without these impurities, e.g. the HC samples in Table 1, transmission down to 200 nm is common.

Samples A and B exhibit similar transmittance behavior, which is expected as a result of their similar % air and capillary size. Sample C shows increasing transmittance with wavelength increase outwards from the visible light region. This is also an expected result, as the sample appears black (in the visible) and is therefore likely to absorb less at longer

wavelengths. The transmission of sample D exhibits oscillatory behavior, and we anticipate that this is due to diffraction. The capillary size is very small compared to the other samples, and only about 1 order of magnitude larger than the operating wavelength. Consequently, slight misalignments of the sample with respect to the source during the test can lead to an effective aperture small enough to cause diffraction. The behavior is less pronounced as the wavelength decreases, which supports this speculation.

3. New Lin Modes Found

New modes suitable for acceleration were found in the 2nd, 3rd, and 5th band gaps for the Lin configuration shown in Fig. 2. Table 2 shows a comparison between these modes and the previously-found, lowest mode discussed in [1]. The real component of the effective index for each mode describes the amount of glass the mode "sees" as it propagates. The imaginary component of the effective index directly relates to mode leakage that should be minimized. As shown in Table 2, one new mode in band 3 has a significantly lower n_{im} value than the fundamental Lin mode.

Also displayed in Table 2 is the ratio of $E_{z,maxcore}$ to $E_{z,maxglass}$ for the 6, 7 and 8 ring cases of each Lin mode. This figure of merit, called $E_{z,n}$, is important because it describes the efficiency of the system or gradient capacity. The lowest mode has the highest value with 62%, and the ratio generally decreases with band increase. We estimate that the ratio from band 2 ($\approx$50%) is acceptable.

One way to decrease n_{im} for any configuration is to add rings, as demonstrated in Table 2. The decrease in n_{im} vs. number of rings was plotted for the Lin mode. This is shown in Fig. 15. A second-order polynomial fit was obtained by assuming a linear correction factor α and a quadratic correction factor β in the following two relations:

$$
\begin{aligned}
n_{i7} &= n_{i6} + \alpha + \beta \\
n_{i8} &= n_{i6} + 2\alpha + 4\beta
\end{aligned} \tag{1}
$$

For the Lin Mode, we calculated α and β to be $-1.28 \cdot 10^{-4}$ and $-1.22 \cdot 10^{-5}$, respectively. This suggests that there is very little gain in going beyond 7 or 8 rings.

The discovery of the higher-order accelerating modes in the Lin configuration has extensive implications. Most importantly, it has been shown that excitation wavelengths can vary significantly for a given fiber. For example, in Table 1, the Lin configuration has been shown to support acceleration modes over at least 450 nm $\leq\lambda\leq$ 1000 nm. This implies larger defects and capillary sizes may be practical to use. It also means that the type of laser used to excite the mode can vary. With a tunable laser source, different accelerating modes could be generated with minimal delay. Also, if a certain excitation wavelength were desired, several different (appropriately scaled) structures could be built specifically for that wavelength. For example, it should be noted that no fiber can currently be produced to the Lin specifications. Fabricating fibers with a defect radius of 2.5 μm is more realistic. By scaling the values to this design, we found that the center wavelength of the operational band is about 1.65 μm.

4. Incom Sample Mode Search

After several CUDOS trials, no modes suitable for acceleration were found in the first or second gaps for Incom B, even though the band gap diagram indicates that such modes may exist. More searches with smaller wavelength increments may result in useful modes. It is also possible that no accelerating modes exist in these bands, even though the bands cross the SOL line. This suggests that the likelihood of finding these modes is very sensitive to defect size in relation to the lattice. One goal is to develop a procedure for how to perturb such lattices to bring the required modes into these gaps.

Both the first and second bands of the diagram for Incom D were found to support defect modes, as shown in Figures 10 and 12. The effective index components and $E_{z,core}/E_{z,glass}$ ratios for these two modes are given in Table 3. The lowest mode strongly resembles the Lin mode, and this is reasonable. Incom D and the Lin configuration have very similar capillary radius to pitch ratios, as well as defect radius to pitch ratios. In fact, the lowest-order Incom D mode has comparable effective index values compared to the Lin mode, but also a slightly better E_z ratio. It's field distribution also compares favorably, as shown in the next figures (11, 13, 14).

For the Incom D case, the lowest-order mode shows TM_{01} nature in Fig. 11; it is uniform, radially symmetric over the defect region, and falls off smoothly with reduced amplitude outside. Alternatively, the second-band mode (shown in Fig. 12) shows very clear TM_{02} characteristics, with a uniform and radially symmetric field in the defect region, as well as a second peak of comparable amplitude in the lattice. It is important to note that these only show absolute E_z. Horizontal (x) and vertical (y) slices of E_z from the center outward for each of these modes are given in the figures. For comparison, a similar picture for the lowest-order Lin mode is given in Fig. 14. The outer edge of the defect is clearly shown in these plots. Note that Lin describes his mode as TM_{0l}-like. By comparison, it appears more TM_{03}-like.

5. Outlook

Although several types of PBG fibers are available, most are not suitable for a particle acceleration application. For example, telecom fibers are made for TEM mode applications. Very small capillaries in new PBG samples should allow us to work at wavelengths that were previously impossible.

In our application, one figure of merit for PBGs is the ratio of central defect size to operating wavelength. This value should be maximized to reduce damaging effects of high-energy electrons traveling down the fiber. The Lin configuration utilizes a wavelength on the order

of the defect size, which is impractical. A yet-to-be discovered configuration that employs a much larger defect size to wavelength is required for practical PBG fiber acceleration that does not compromise accelerating gradient. One avenue toward this goal is a more detailed tailoring of the outer periphery of the defect and near lattice in terms of shape and material.

VI. REFERENCES

[1] X.E. Lin. "Photonic band gap fiber accelerator," Physical Review Special Topics - Accelerators and Beams Vol. 4 051301 May 2001

[2] Several samples were provided to us by Jeffrey Solari of Incom, Inc. www.incomusa.com

[3] CUDOS Microstructured Optical Fiber Utilities http://www.physics.usyd.edu.au/cudos/mofsoftware/

[4] RSOFT BandSOLVE www.rsoftdesign

[5] Varian Inc. Cary 5000 NIR Spectrophotometer www.varianinc.com

[6] T.P. White, B.T. Kuhlmey, R.C. McPhedran, D. Maystre and G. Renversez, C. Martijn de Sterke, L.C. Botten. "Multipole method for microstructured optical fibers," J. Opt. Soc. Am. B, Vol. 19, No. 10, Oct. 2002

VII. ACKNOWLEDGMENTS

This research was conducted at Stanford Linear Accelerator Center. The author would like to recognize the U.S. Dept. of Energy, the Office of Science, and SLAC for organizing and funding the SULI program. Special thanks are extended to Bob Noble and Jim Spencer for their encouragement and guidance.

FIGURES

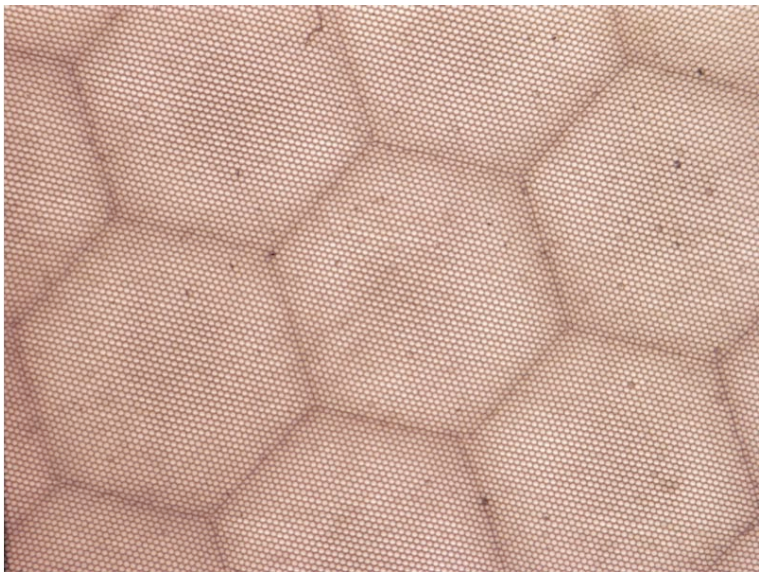

Figure 1: Incom sample D Photonic Band-Gap lattice.

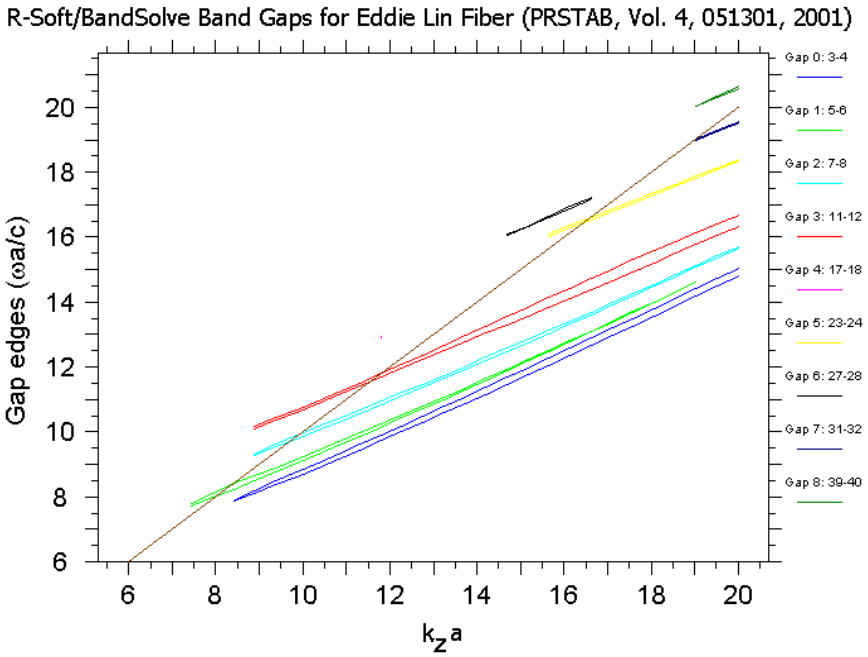

Figure 2: Complete band gaps for the Lin configuration (Table 1).

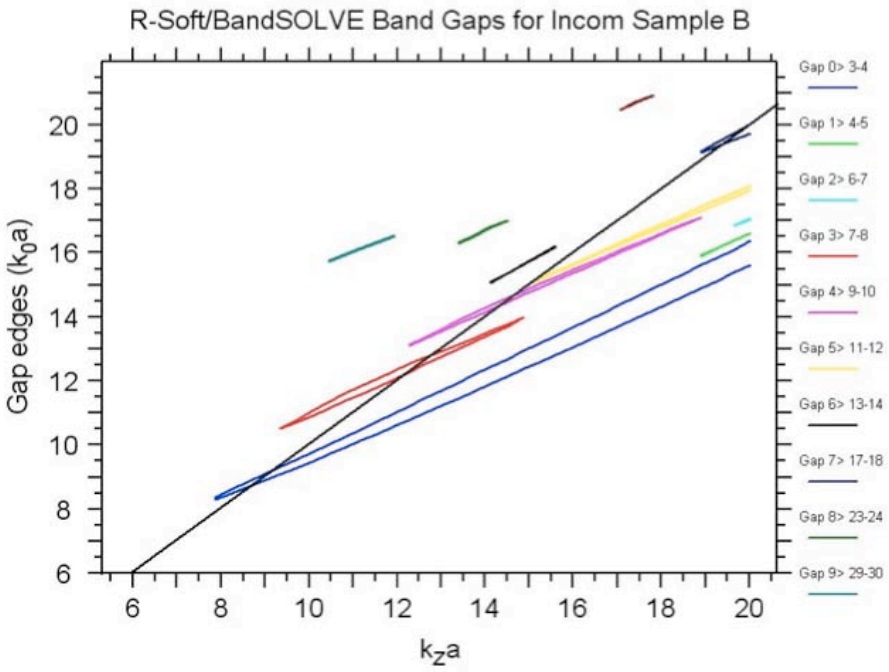

Figure 3: Unperturbed lattice band gaps of the Incom B PBG sample (Table 1).

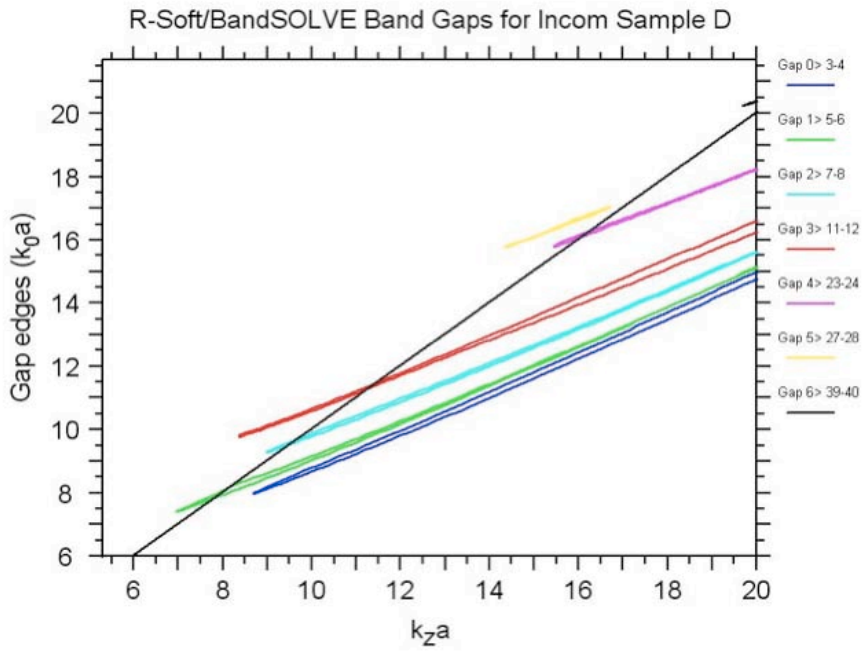

Figure 4: Unperturbed lattice band gaps of the Incom D PBG sample (Table 1).

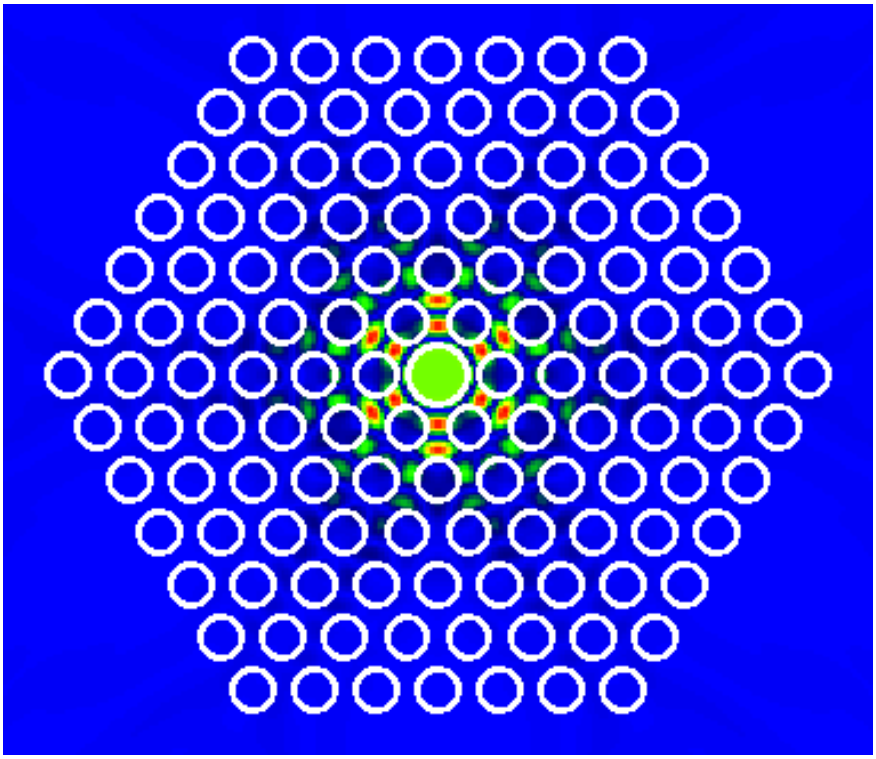

Figure 5: E_z for the lowest-order mode of the Lin configuration.

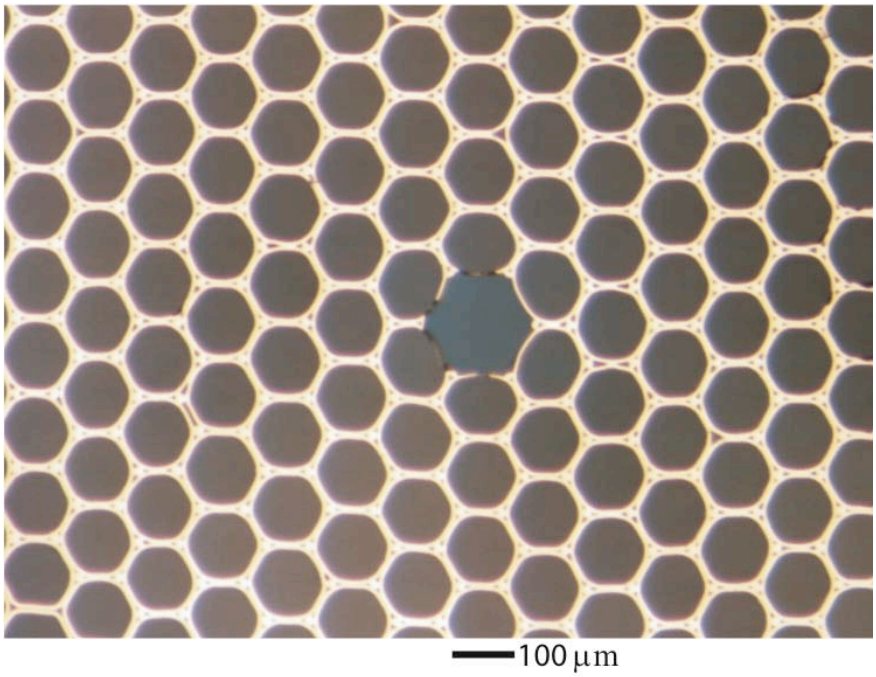

Figure 6: Photo of a 100μm PBG lattice (Incom B) with single capillary defect.

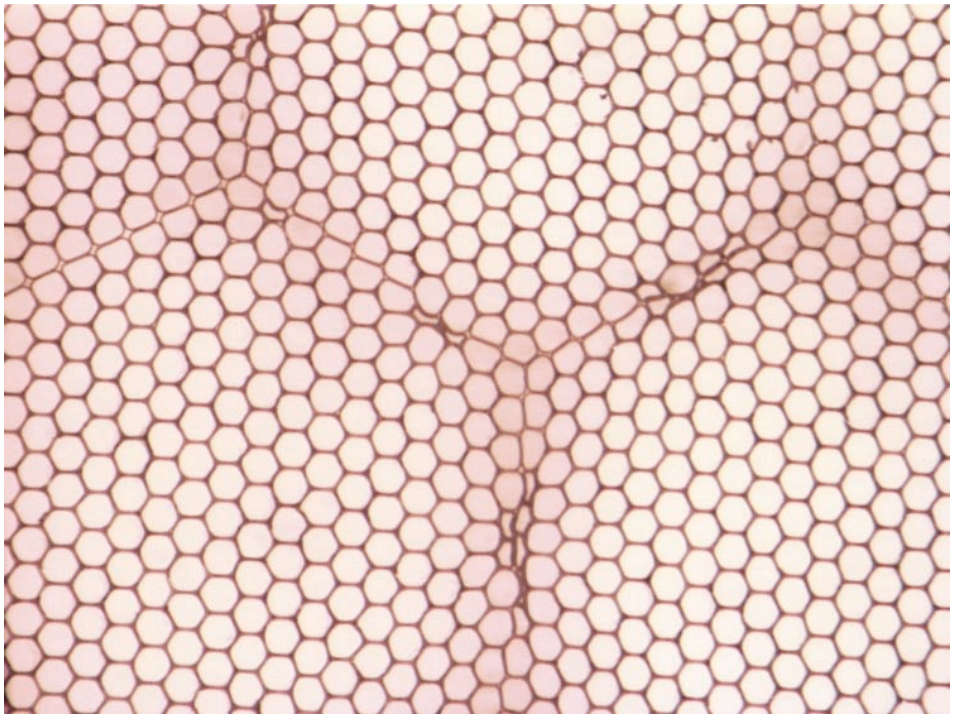

Figure 7: Construction errors along larger super-hexagonal lattice (Incom A).

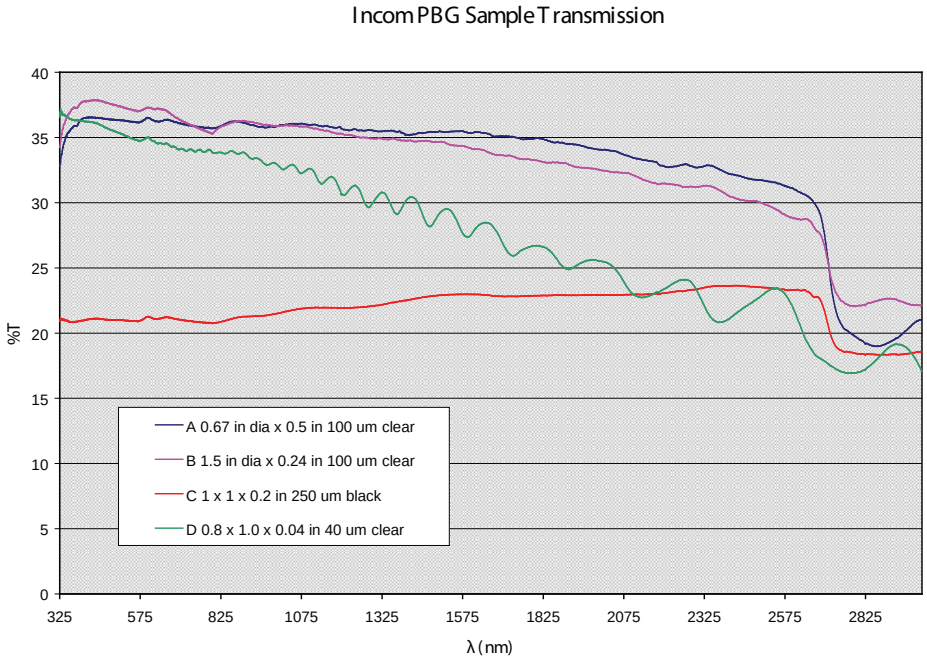

Figure 8: Transmittance data for the Incom samples.

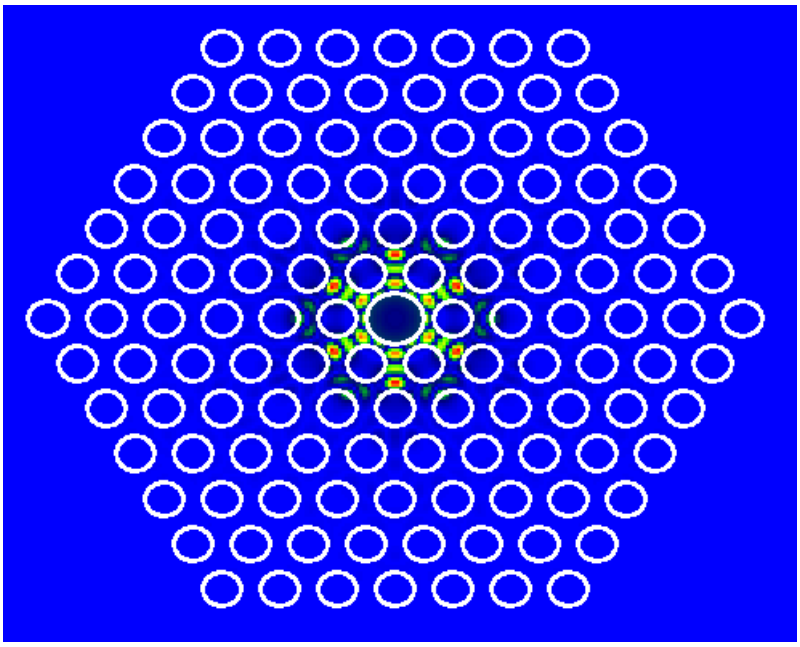

Figure 9: E_z for a third-band mode of the Lin configuration.

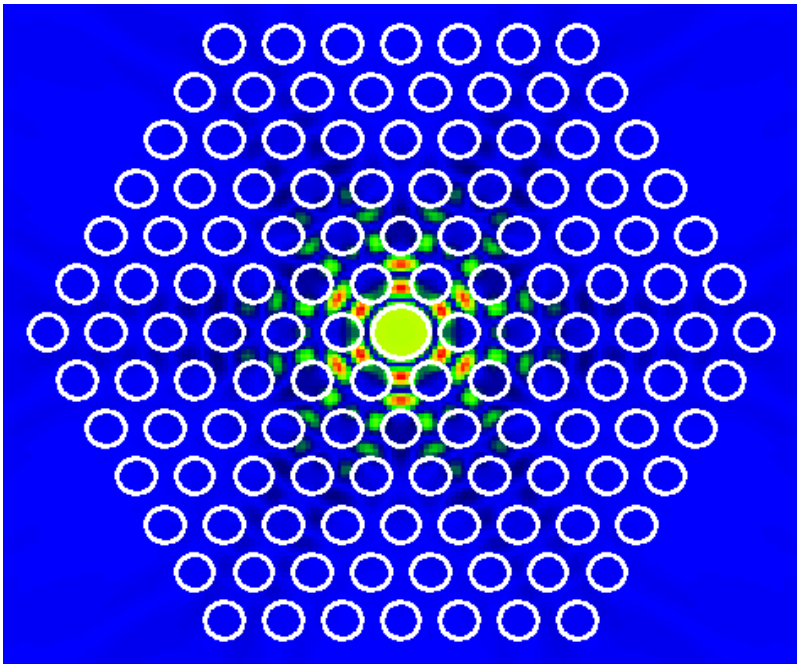

Figure 10: E_z for a first-band mode of the Incom D sample.

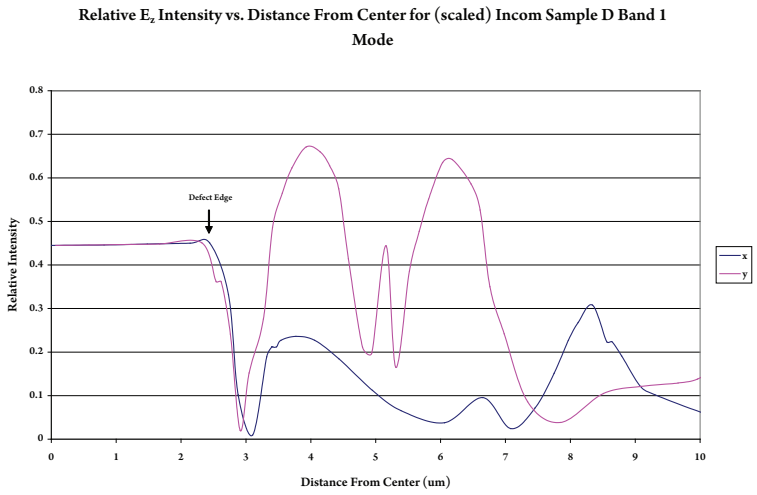

Figure 11: Intensity vs. distance from defect center for the Incom D Band 1 mode.

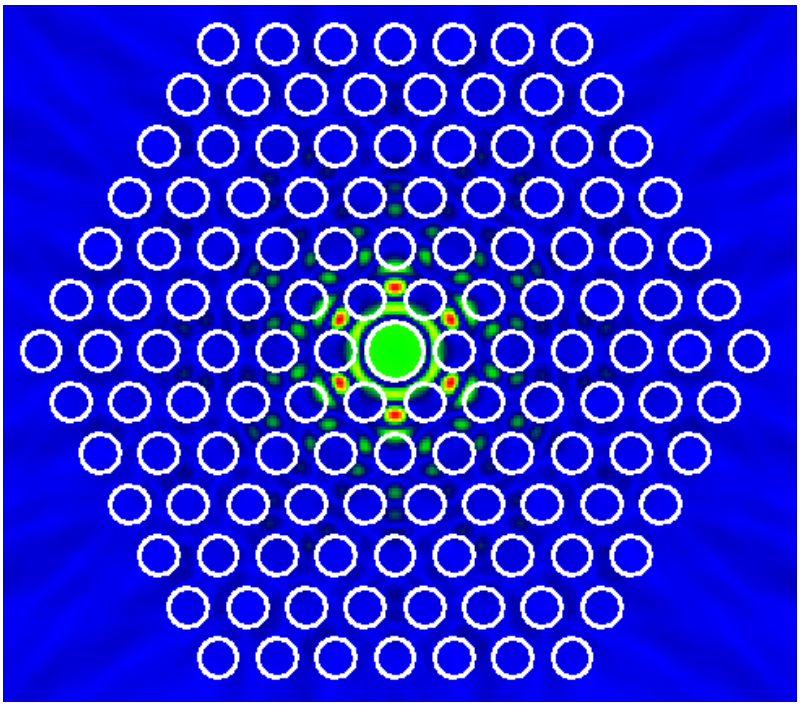

Figure 12: E_z for a second-band mode of the Incom D sample.

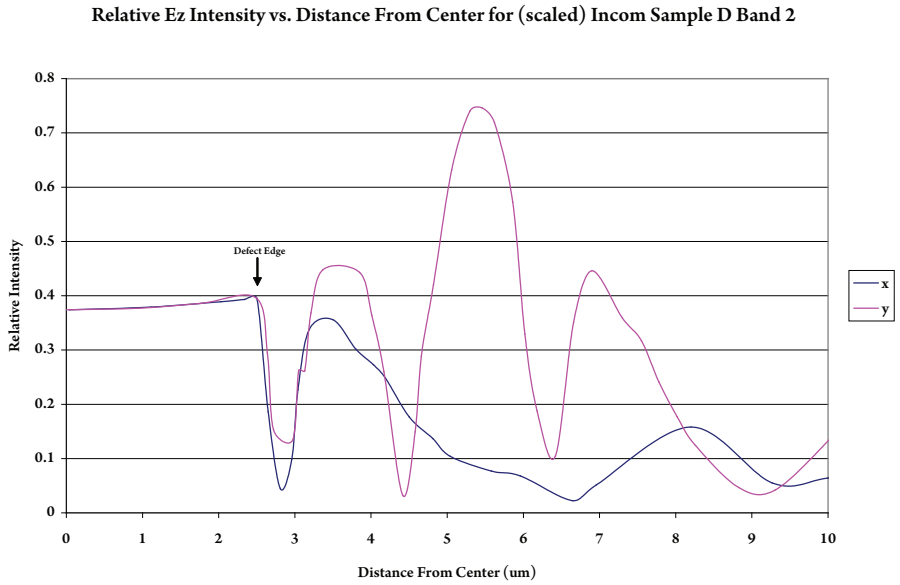

Figure 13: Intensity vs. distance from defect center for the Incom D Band 2 mode.

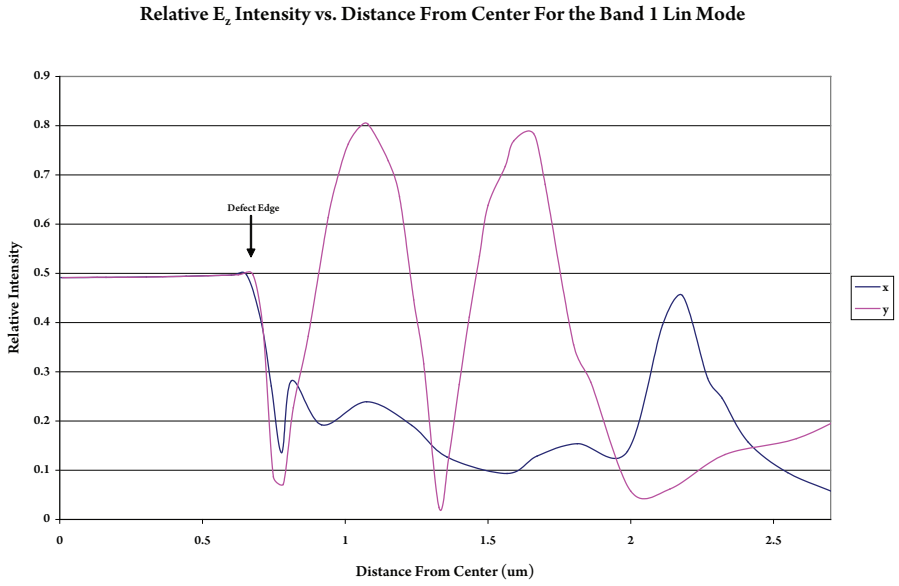

Figure 14: Intensity vs. distance from defect center for the lowest-order Lin mode.

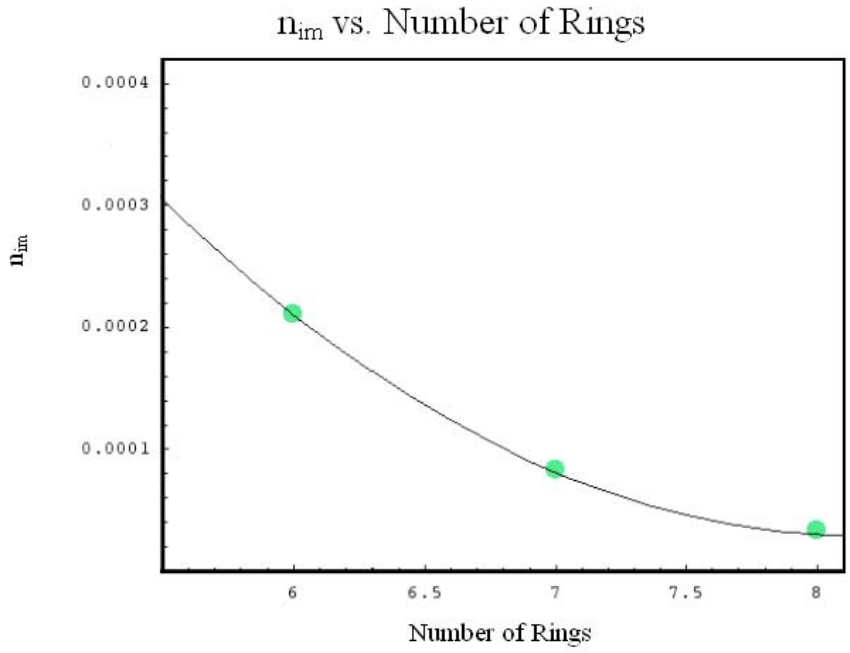

Figure 15: Imaginary effective index vs. ring number for the lowest-order Lin mode.

TABLES

TABLE 1. Representative examples and their characteristics for silica (ϵ=2.13) PBG fibers.

Parameter	$\mathbf{N}_{Def}$[1]	$\mathbf{N}_{Rgs}$[2]	**Wavelength** [nm]		**Pitch**	$\mathbf{R}_{Def}$	$\mathbf{R}_{Air}$	% **Air**	**Qual.**[3]
Designation	#	#	Center	Trans.Bd	μm	μm	μm	%	#
HC-1550-02[4]	7	9	1550	>200	3.8	5.45	–	>90[5]	1
HC19-1550-01	19	9	1550	>80	3.9	10±1	–	>90	2
HC-440-01	7	9	440	>60	1.44	2.45	–	>90	3
X.E. Lin[6]	1	6	1000	>20	1.31	0.68	0.46	65	–
Incom-A[7]	–	–	–	–	122.2	–	55	86.9	3
Incom-B	–	–	–	–	113.6	–	50	84.7	3
Incom-C	–	–	–	–	391.9	–	125	73.4	1
Incom-D	–	–	–	–	58.65	–	20	63.6	2

[1] Number of missing capillaries constituting the defect.
[2] Number of included capillary rings – excluding the single capillary for a perfect lattice.
[3] Qualitative measure of construction uniformity with "1" being best.
[4] www.blazephotonics.com for telecom apps based on amorphous, fused quartz (Suprasil).
[5] Excludes central defect core and outer ring of holes.
[6]X.E. Lin, "Photonic band gap fiber accelerator", Phys. Rev. ST Accel. 4(2001)051301. Calculated results.
[7] www.incomusa.com uses borosilicate "pyrex" and other glasses have very similar characteristics to a-SiO_2.

TABLE 2. Lin mode effective index comparison by number of rings. ($E_{z,n} = E^{max}_{z,Def}/E^{max}_{z,glass}$)

Mode	$\lambda(\mu$m)	$\mathbf{n}_{re,6}$	$\mathbf{n}_{im,6}$	$\mathbf{E}_{z,6}$	$\mathbf{n}_{re,7}$	$\mathbf{n}_{im,7}$	$\mathbf{E}_{z,7}$	$\mathbf{n}_{re,8}$	$\mathbf{n}_{im,8}$	$\mathbf{E}_{z,8}$
1, 1	1.008	1.001	$2.11 \cdot 10^{-4}$	0.62	1.001	$8.34 \cdot 10^{-5}$	0.64	1.001	$3.45 \cdot 10^{-5}$	0.64
2, 1	0.839	1.005	$1.69 \cdot 10^{-3}$	0.502	0.972	$1.05 \cdot 10^{-3}$	n/a	1.005	$7.48 \cdot 10^{-4}$	0.30
2, 2	0.839	1.005	$1.69 \cdot 10^{-3}$	0.502	1.005	$1.07 \cdot 10^{-3}$	0.503	1.005	$7.48 \cdot 10^{-4}$	0.50
3, 1	0.690	1.012	$5.72 \cdot 10^{-5}$	0.279	1.012	$3.41 \cdot 10^{-5}$	0.31	1.0012	$1.75 \cdot 10^{-5}$	0.30
3, 2	0.690	1.005	$7.26 \cdot 10^{-4}$	0.324	1.004	$4.52 \cdot 10^{-4}$	0.243	1.005	$4.31 \cdot 10^{-4}$	0.302
3, 3	0.690	1.007	$1.21 \cdot 10^{-3}$	0.34	1.006	$9.15 \cdot 10^{-4}$	0.299	1.007	$8.84 \cdot 10^{-4}$	n/a
5, 1	0.450	1.008	$3.69 \cdot 10^{-4}$	0.229	1.000	$2.50 \cdot 10^{-4}$	0.270	1.000	$2.66 \cdot 10^{-4}$	0.238

TABLE 3. Incom D Modes.

Band	$\lambda(\mu\mathrm{m})$	$\mathbf{n}_{re,6}$	$\mathbf{n}_{im,6}$	$\mathbf{E}_{z,6}$
1	3.93	1.0018	$3.223 \cdot 10^{-4}$	0.68
2	3.27	1.005	$2.25 \cdot 10^{-3}$	0.523